STUDIA UBB CHEMIA, LXX, 3, 2025 (p. 243-263)
(RECOMMENDED CITATION)
DOI:10.24193/subbchem.2025.3.17

HYDROTHERMAL CO-LIQUEFACTION OF PROSOPIS JULIFLORA AND POLYPROPYLENE IN CONTINUOUS HIGH PRESSURE SCREW REACTOR: A COMPUTATIONAL AND EXPERIMENTAL ANALYSIS

Chitra Devi VENKATACHALAM[a*], Premkumar BHUVANESHWARAN[a], Mothil SENGOTTIAN[b], Sathish Raam RAVICHANDRAN[b]

ABSTRACT. In advancement over batch reactors for biomass conversion, a continuous high-pressure screw reactor was designed to perform hydrothermal co-liquefaction (co-HTL) under a range of conditions: temperatures of 555–595 K, water-to-biomass ratios (W/B) of 6.3–8.3, and feed rates of 0.005–0.0085 kg/s. *Prosopis juliflora* (PJ) and polypropylene (PP) were used in biomass ratios of 1:4, 1:1, and 4:1. Computational Fluid Dynamics (CFD) using ANSYS Fluent was employed to analyze heat transfer between the reaction chamber and slurry biomass. For 595 K, 8:3 W/B, and 0.007 kg/s, the simulation predicted a maximum temperature of 589.3 K and pressure of 22.1 MPa, showing a 1.3 MPa deviation from experiments due to low-density particles and higher process temperatures. The simulated heat transfer coefficient was 6001 W/m^{2}K, matching experimental data with 94.6% accuracy. Under these conditions, energy recovery reached 70.8%, with biochar and biocrude yields of 34.2% and 48.7%, respectively. A synergistic effect in biocrude and biochar production was observed at a 4:1 PJ:PP ratio, independent of temperature. GC-MS analysis confirmed major aromatic hydrocarbons, including 1-[(E)-2-(4-chlorophenyl)ethenyl]-3,5-dimethoxybenzene, 2-methoxyphenol ($C_7H_8O_2$), and phenol (C_6H_5OH). The optimal conditions of 595 K, 8:3 W/B, and 0.007 kg/s are recommended for maximum energy recovery and efficient heat transfer.

Keywords: *High-pressure screw reactor, Hydrothermal Co-liquefaction, Prosopis juliflora, Polypropylene, heat transfer, energy conversion.*

[a] *Department of Food Technology, Kongu Engineering College, Erode-638060, Tamil Nadu, India*
[b] *Department of Chemical Engineering, Kongu Engineering College, Erode-638060, Tamil Nadu, India*
* *Corresponding author: erchitrasuresh@gmail.com*

INTRODUCTION

Hydrothermal co-liquefaction (co-HTL) is one of the most promising thermochemical conversion processes to understand the synergistic effect of combined biomass. It also provides enhanced conversion rates and divergent bio-energies. Since then, numerous studies have been conducted on various hydrothermal reactors, including Parr micro bench top reactors, high-pressure autoclave reactors and continuous bench scale reactors to determine the quality and energy efficiency of the bioproducts. It is important to upgrade the bench to pilot-scale reactor for commercializing bioenergy without changing its chemical properties [1-4]. Initially, the continuous plug flow reactor is used for pilot scale operation with a capacity of 6-14 kg/h, which gives a maximum biocrude yield of 33 wt.% and also a higher energy recovery than the bench-scale reactor. However, the plugging of slurry biomass is the major reason for uneven radial mixing and pressure drop in the reactor, which also affects the mass flow rate and biomass reactions during the hydrothermal process [5-7]. In addition, a smaller length-to-diameter ratio, rapid mixing of biomass and faster reaction rate are the major drawbacks explored in the continuous plug flow reactors [8]. Therefore, recent studies have given more attention to continuous pilot-scale operations in both screw and non-screw thermal reactors for the co-HTL process.

The Pacific Northwest National Laboratory (PNNL) has developed a continuous flow reactor equipped with a booster pump, a pre-heater, an agitator and a 1L tubular reactor to treat sewage sludge, achieving a flow rate of 1.5 L/h for a continuous operation of 6 to 10 h. It approximately produces 80% of the carbon recovery and 25% of the maximum biocrude yield [4, 9]. Similarly, a small tubular reactor with a capacity of 50 mL was loaded with alkaline pretreated biomass at 475 K and a mass flow rate of 20 kg/h. Then, the biomass was reacted at 675 K and elevated to a high pressure of 30 MPa during 4 hours of continuous operation. It resulted in a 10% higher biocrude yield than the non-pretreated biomass. Additionally, it was found that the higher heating value (HHV) and carbon recovery of bio-crude in continuous tubular operation were comparatively lower than in micro-scale batch operation [10, 11]. A.R. Suesse et al. [12], developed a pilot-scale supercritical flow reactor (SCFR) operated at a maximum temperature and pressure of 725 K and 65 MPa, respectively. It consists of a ten-liter paddle mixer to ensure a homogeneous mixture of slurry biomass, a plunger pump for transporting the mixture to the preheater and a heat exchanger. The optimum biocrude yield of 70% and calorific value of 36.4 MJ/kg were achieved at 575 K similar to the tubular reactor [12]. Instead of a mechanical pump, the feed was also delivered into the inner chamber of the vertical double-tube reactor at

a flow rate of 3 to 7 mL/min using pressurized nitrogen of 16 MPa. The reactor was heated to the maximum temperature of 625 K and placed in the tubular furnace. As a result of the higher heating rate and retention time, the biocrude yield was improved compared to the batch system, and the hotspot regions on the reactor wall were also reduced. [13, 14]. These studies reveal that the mixing of waste sludge and heat transfer rate is not efficient in screwless continuous flow reactors and also not effective to produce a significant amount of bioproduct yield and energy recovery. A longer retention time also leads to thermal cracking.

A pilot-scale reactor was developed with a hydraulic oscillation system having an internal volume of 20 L and a maximum feed rate of 100 L/h to increase the turbulence during the reaction. The oscillation mechanism also supports better mixing and heat transfer, but does not improve the quality of the bioproducts. The average bio-crude yield of 33 wt.% occurred for 5 to 6 h residence time and achieved 80% heat recovery in the heat exchanger. However, a lower HHV of 26-33 MJ/kg was obtained compared to other continuous processes [5, 15]. Two continuous screw reactors of five-liter internal volume were developed for hydrothermal processing of pre-treated lignocellulosic biomass. The compressed hot water was used to heat the reactors to reach the steady state. Thereafter, the slurried biomass replaces the hot water at a flow rate of 9 to 14 kg/h using a high-pressure piston pump (30 MPa) to promote biocrude production. The recirculation of hot water occurs at the end of each batch process, which tends to reduce the yield of bio-crude and causes significant disruption due to fouling during the process [16]. In some cases, deionized water was supplied under pressure to heat the reaction chamber, after which it was replaced by biomass slurry using a feed pump [17]. Mostly, high-pressure feed pumps and piston pumps for continuous feed mechanisms are developed to inject biomass into the reaction medium at a process rate of 16.9% to 17.5%. As a new experimental study, the performance of a high-pressure screw reactor with three pressure development zones was used in the present study to eliminate the mechanisms of preheating, oscillation and recirculation.

An efficient heat transfer is a vital phenomenon to enhance the performance of any thermochemical conversion reactor. Accordingly, some computational fluid dynamics (CFD) models were employed to investigate the heat transfer behaviors between solid-solid and solid-fluid particles. In specific, Moving Mesh Motion (MMM) and Rotating Frame Motion (RFM) are the fluent simulation models used to perform the screw rotation [18-20]. Similarly, Euler-Euler, Euler-granular and Euler-Lagrangian were important cell-based numerical approaches to study the interaction between the different phases using appropriate governing equations such as continuity, momentum and kinetic

energy in continuous multi-phase flow media. Newton's law of motion supports the numerical models for describing the motion and the additional forces acting between the solid and fluid phases during the co-HTL process. These equations ensure homogeneous mixing, mass balancing and smooth transportation of the slurry biomass, depending on the screw diameter, thickness, helix angle and flight length. Further, kinetic energy equations are utilized to predict the thermal properties, including temperature and pressure distribution, viscosity, heat transfer coefficient (HTC) and heat flux during the fluid flow [18, 19, 21, 22].

Most studies have related reactor performance in terms of chemical composition, heating value and energy recovery of the biofuels produced. In particular, the HHV determines the efficient state of any fuel, which can be evaluated using the elemental compositions (C, H, N, S, O) present in the biofuels. The correlations obtained from the prediction model was applied to calculate the HHV [23-26]. The H/C and O/C ratios are estimated from elemental composition and plotted in the Van Krevelen diagram to represent the quality of bioproducts [27]. In addition, the direct HHV of the biomass, biosolids and bioliquids was also measured using the oxygen bomb calorimeter. Hence, the total energy recovery and the mass balance are crucial for describing the energy intensification, thermal degradation of biomass and the performance of the reactor [19, 21, 28, 29].

In the present study, heat transfer analysis was performed on a continuous high-pressure screw reactor using suitable governing equations in the CFD module. Further, the performance of the screw reactor was also investigated based on yield, HHV and energy recovery of bioproduct.

RESULTS AND DISCUSSION

Heat transfer studies

The simulation was performed for a flow duration of 10 s to reduce the complexity of convergence. The steady state condition was observed in the fluent simulation based on the iteration graph, then the CFD results were obtained between cylindrical casing and slurry biomass.

Pressure vs temperature variation

It discloses the maximum temperature occurred at the outer region and decreased radially towards the inner region of the reaction chamber. The experimental observation also confirms that the slurry biomass was highly converted in the outer region and lesser towards the inner region, which shows the uniform heat transfer towards the inner region of the reaction chamber.

Fig. 1 shows that run-8 has the highest simulation temperatures of 589.3 K and 494.3 K at the outer and inner regions of the reaction chamber, which were approximately 10.3 K and 10.7 K deviated from the experimental temperatures for the given process condition. Likewise, the maximum pressure and its deviation from the experimental value occurred in run-8 as 22.10 MPa and 1.3 MPa, respectively. It shows the direct proportionality between pressure and temperature.

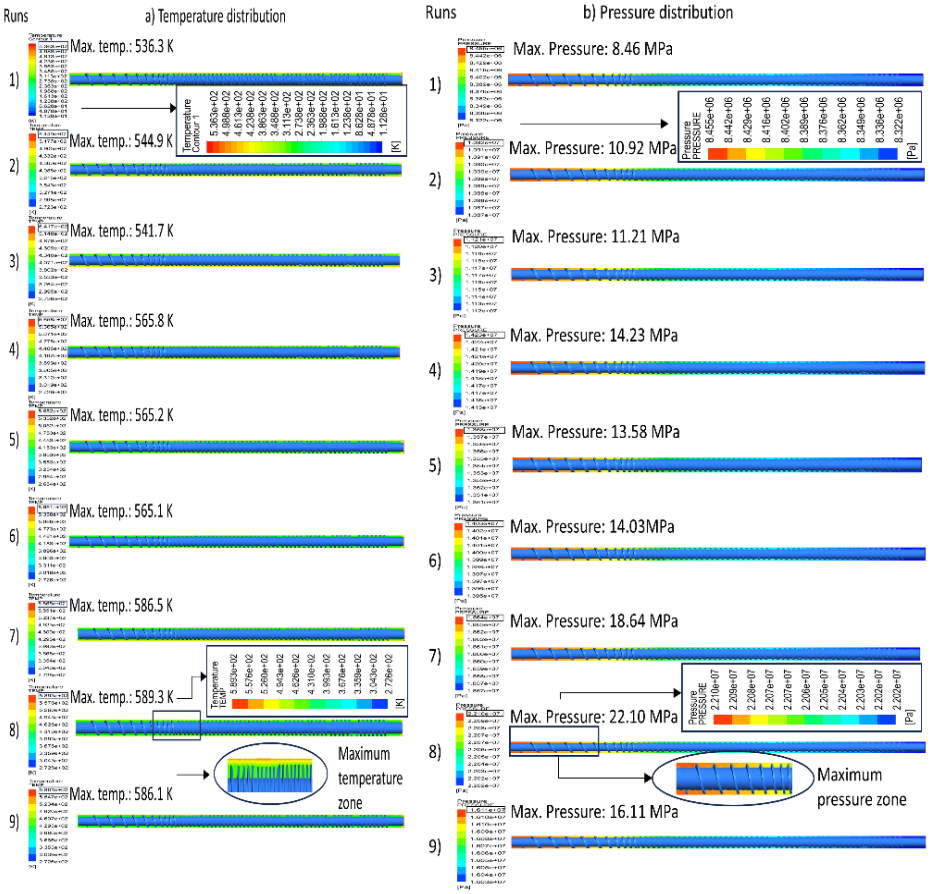

Figure 1. Contour plot for a) temperature and b) pressure distribution after reaching steady state conditions

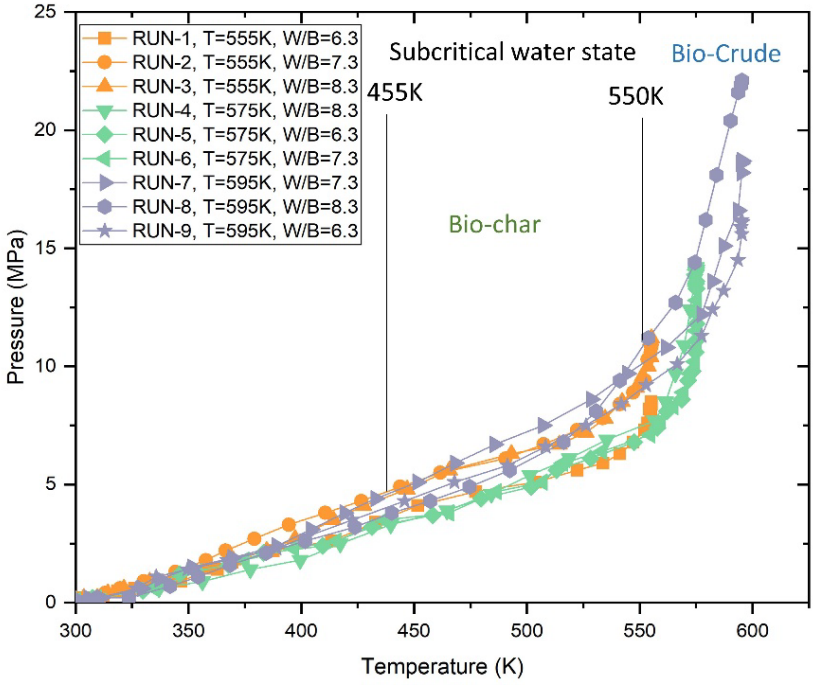

Figure 2. Relationship between temperature and pressure for respective process conditions

The relation between temperature and pressure with respect to water-to-biomass ratio is shown in Fig. 2. The co-HTL process was conducted under temperatures between 555K and 595K at subcritical water state, which provides the fast and efficient reaction medium to developed the autogenous pressure ranges from 8.46 MPa to 22.1 MPa. In addition, Fig. 2 revealed that water-to-biomass ratio plays a vital role in pressure development besides temperature and mass flow rate. The higher pressure was observed particularly for water-to-biomass ratio at 8.3 with their corresponding temperatures. In subcritical condition, the high amount of ionic product from water accelerated the biomass hydrolysis and mostly favor to form the biocrude rather than biochar. It was noticed at the temperature above 575K as given in Fig. 2.

Fluctuations of temperature

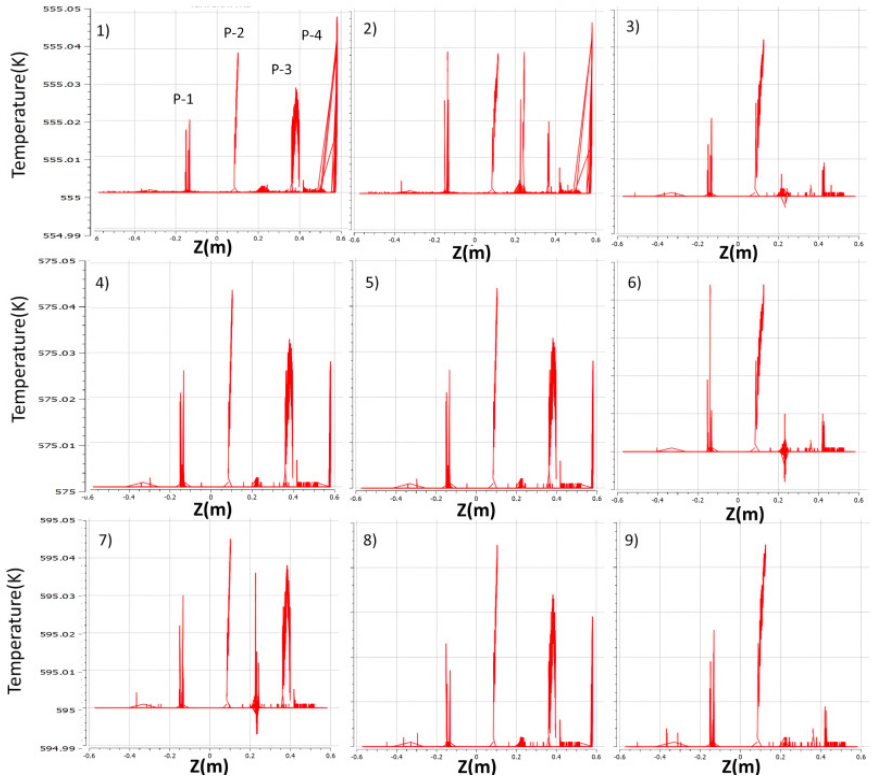

Figure 3. Fluctuation of maximum temperature on the cylindrical casing of the reactor along the axial direction

Fig. 3 confirms the process temperature maintained at the cylindrical casing throughout the length of the reactor. A very slight deviation was observed closer to each compression zone CZ-1, CZ-2 and CZ-3 for flow duration of 1s in fluent simulation. It will be higher for increasing the flow duration in simulation. Runs 1-9 possess a slight deviation of 0.05 K in simulation and a deviation range from 20K to 30K in experiment was noticed that occurs due to the friction caused between the restricted flow in compression zones and the cylindrical casing. The peak temperatures denoted as P-1, P-2, P-3 and P-4 raised at different lengths of the reaction chamber, mentioned as 450 mm, 680 mm, 1000 mm and 1160 mm, shown in Fig. 8. Owing to the high restriction of biomass, the peak P-2 shows the highest deviation that occurs before CZ-2 compared to other peaks observed in each run. In experimental conditions,

a noticeable amount of clogging was observed at the intersection of the expansion and CZ-1 zones. However, the maximum process temperature was maintained in the remaining zones of the reaction chamber.

Actual and Predicted HTC

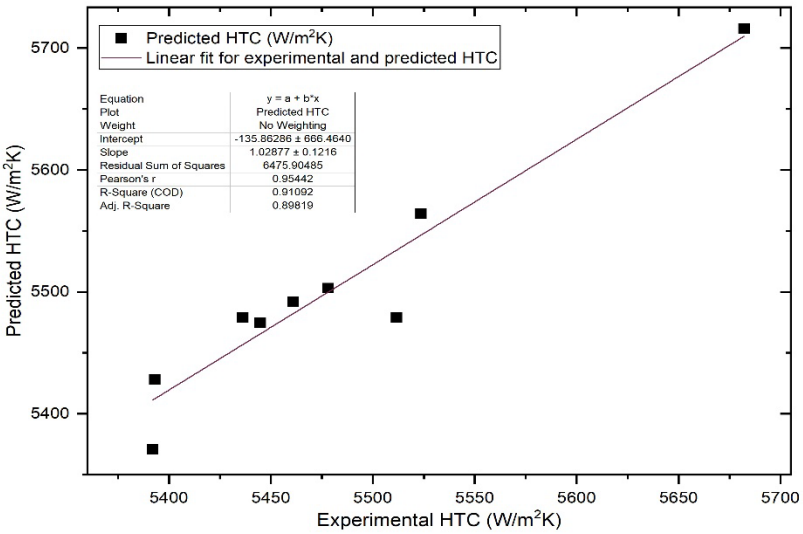

Figure 4. Comparison of HTC between predicted and experimental results

Fig. 4 shows that the predicted results were linearly fitted to the experimental data. It also delivered a wide range of mean deviation between the predicted and experimental results from 4.2% to 6.85%, with a maximum error value of 44 W/m2K. The Root Mean Square Value (RMSE) of the present model was estimated as 33.22 %, which is comparatively less than the Yan et al.[30] correlation for predicting HTC with the RMSE of 64.2%. It is slightly higher than the RMSE of 32 % calculated in the Longo et al.,[31] model, which has 93% accuracy in HTC prediction due to larger data collection [31]. From the adjusted R-squared value, it is observed that the predicted value possessed an average accuracy of 89.8% with the experimental values. The HTC of runs 3, 7, 8 and 9 nearly fitted with the linear regression line and possessed a minimum slope. In contrast, runs 2, 4 and 6 have more deviation from the regression line with a higher slope. The predicted HTC results were always higher than the experimental results due to significant heat loss among cylindrical casing, slurry biomass and ambient conditions. In addition, the variation in biomass thermal properties due to their temperature difference led to a decrease in the experimental HTC during the reaction.

Reactor Performance Analysis

The bioproduct yield, HHV and energy recovery are the vital response parameters considered to analyze the performance of the high-pressure screw reactor. In addition, the co-liquefaction effect was calculated to understand the effect of biomass mixture in the reactor and GC-MS was carried out to investigate the thermal degradation of volatile compounds present in the biocrude.

Bioproducts yield

The HTL of PJ in a 250 mL auto batch reactor provided the maximum bio-crude yield of 42.5% at 700 K. The higher conversion of biogas was observed for further increasing the temperature [32]. A similar operation was performed in a 600 mL autoclave batch reactor, which delivered the maximum biochar and biocrude yield of 45.7% and 45.82% at 525 K [33]. In subcritical temperature (below 625 K), the highest yield of biochar 58.6 % was obtained with bio-crude residue of 15.2 % at 615 K [34, 35]. Chen et al.,[36] found that the optimum yields of 37.5% and 58.6% were attained for corresponding bio-crude and biochar at supercritical temperatures of 695 K and 655 K, respectively [36]. The Liquefaction of PP at 625 K provides the highest biochar yield of 92% with a slight biosolid residue of 6%. Meanwhile, further temperature increases, abruptly decreased the bio-crude and biochar yield to 36% and 2% [34].

The present study compares the bioproduct yield attained from the co-liquefaction of PJ and PP with the optimum yield from HTL of PJ and PP, as depicted in Fig. 5. The highest biochar yield of 45.3% and bio-crude of 53.2% were attained for the corresponding water-to-biomass ratio of 6.3 and 8.3 at 555 K. Run-8 possesses a biochar and bio-crude yield of 35.2% and 48.7 % at 595 K. It stated that the bio-crude yield was comparatively higher than the yield of PP liquefaction at a temperature between 625 K and 700 K resulting in Swathi Mukundan et al.,[32] and Biller et al., [15]. Due to the higher pressure in the current process, the aforementioned bio-crude yields were significantly higher than the optimum yield (46.5%) achieved from the co-liquefaction of PJ and 25% of PP at 695 K in the batch reactor [32]. The biochar yield of 39.4% at 555 K was slightly higher than the yield obtained from the liquefaction of PJ at the supercritical condition of 695 K. In contrast, the biochar yields obtained from the co-liquefaction of PJ and PP at respective temperatures were not as high as the optimum yield from PP liquefaction at 625 K as well as PJ liquefaction at the subcritical condition of 615 K. Likewise, a lower amount of biochar was attained from the co-liquefaction of PJ and PP than from the liquefaction of PJ, but it favored the bio-crude yield. In the continuous co-liquefaction process, the quantity of biogas and AqP was

slightly higher than the liquefaction of PJ and PP. It can be gradually decreased by increasing the temperature and pressure of the co-HTL process. The further increase in temperature led to higher pressure generation of 40 MPa, which may affect the system parts and hydraulic fluid tubes in the present hydrothermal reactor. So, the process halted at 595 K.

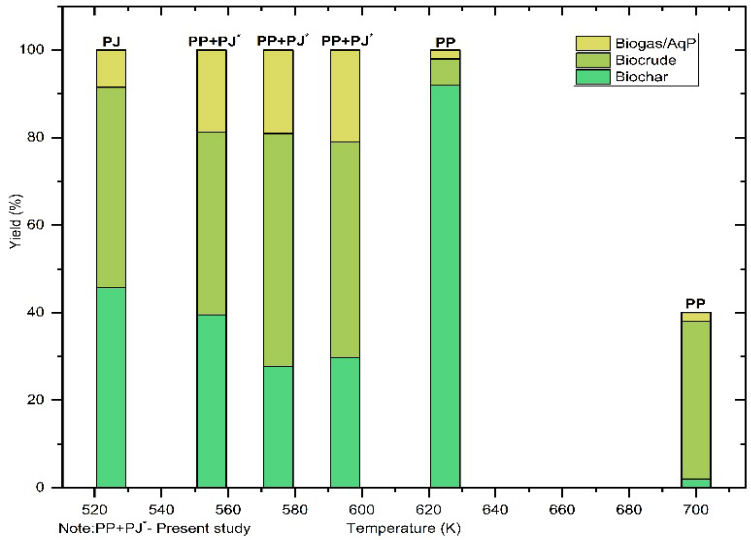

Figure 5. Comparison of maximum yield obtained from co-HTL of PJ and PP at temperatures 555 K, 575 K and 595 K with optimum yield from HTL of PJ and PP

Energy recovery

Figs 6a and 6b illustrate the fluctuation of energy recovery for respective temperatures and biomass ratios. The energy recovery of biochar and biocrude was estimated using corresponding Eqs. (6) and (7). It suggested that the higher energy recovery of biochar and bio-crude was attained at a lower PP ratio in biomass mixture and higher temperature as discussed in the HHV section. The highest energy recovery of 35.16% and 35.64% was calculated for biochar and bio-crude for the corresponding process condition given in run-8. The overall energy recovery was estimated as 70.8% with the standard deviation of 7.8% at similar conditions of biomass ratio and temperature mentioned as 4:1 and 595 K. The lowest overall energy recovery of 54.7% with 8.3 % of deviation was obtained for lower temperature of 555 K and 1:1 biomass ratio. It was observed that the overall energy recovery increased with increasing temperature at a smaller PP ratio in biomass mixture. Similarly, the gradual increase in overall energy recovery was noticed, when increasing the operating

temperature at 1:1 biomass mixture as shown in Fig. 6b. The biochar possessed significantly higher energy recovery than biocrude due to its presence of stable carbon and lower oxygen content.

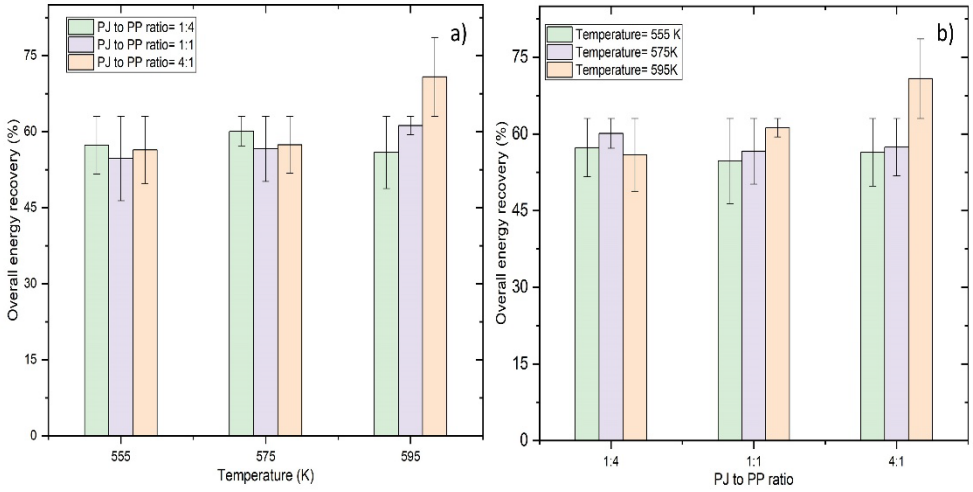

Figure 6. Effect of a) temperature and b) biomass ratio on overall energy recovery of bioproducts

Co-liquefaction effect of PJ with PP

The variation of the co-liquefaction effect related to its temperatures and biomass ratios is depicted in Figs 7a and 7b. The synergetic effect of biochar was observed at lower and moderate temperatures of 555 K and 575 K, respectively and an antagonistic effect was estimated for biochar at a 4:1 PJ to PP biomass ratio irrespective of temperatures. The synergetic and antagonistic effects ranging from 1.37 to 3.53 and -1.11 to -1.14 were noticed in biochar. Run-5 possessed the maximum synergetic effect of 3.53 at 575 k and 1:4 biomass ratio. The lower PP biomass mixture drastically reduced the co-liquefaction value of biochar and showed an antagonistic effect regardless of temperatures. In contrast, the bio-crude has a synergetic effect ranging from 0.6 to 4.78 for given process conditions. Especially, the highest synergistic effect of 4.78 and an antagonistic effect of -1.14 were observed for corresponding bio-crude and biochar at similar process conditions of temperature 595 K and lower PP biomass mixture, as shown in Fig. 7a and 7b. It was slightly higher than the synergetic effect of bio-crude obtained from the co-liquefaction of a 4:1 biomass mixture of sawdust/polyolefin plastic, pistachio hull/polyethylene terephthalate and pistachio/Nylon, which was estimated as 0.7, 3.98 and 3.63, respectively [37-39].

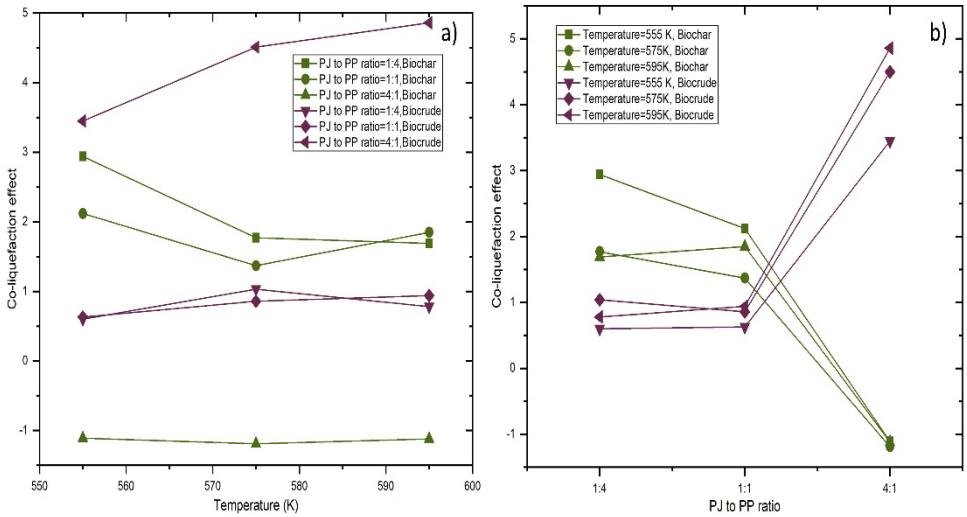

Figure 7. Influence of temperature and biomass ratio on the co-liquefaction effect of biochar and bio-crude

GC-MS analysis

The peak area percentage of selective chemical compounds occupied in the optimal bio-crude. A wide range of aromatic hydrocarbons, ketones and aldehydes were observed in the form of C5 to C17 carbon chains from GC-MS data. The chemical compounds present in the bio-crude were 1-[(E)-2-(4-chlorophenyl) ethenyl]-3,5-dimethoxybenzene ($C_{16}H_{15}ClO_2$), Phenol (C_6H_5OH), 2,3-Dimethoxyphenol ($C_9H_{10}O_4$), 3-Hydroxy-4-methoxy benzaldehyde ($C_8H_8O_3$), Cyclotene (C6H8O2), Cyclohexane 3-ethyl-5-methyl-1-propyl ($C_{12}H_{24}$), 4-Methyl-4-heptanol ($C_8H_{18}O$), Aminocarb ($C_{11}H_{16}N_2O_2$). 2-methyl hexane, Methylcyclohexane and cyclohexane 3-ethyl-5-methyl-1-propyl, which had also been reported by S. Mukundan et al.,[32] and Xiaojuan Zhang et al.,[40]. From the mentioned chemical compounds, aromatic hydrocarbons, Carboxylic acid, oxygenated aromatic hydrocarbons, light oxygenates and a few amino groups were predominantly occupied in the bio-crude. 1-[(E)-2-(4-chlorophenyl) ethenyl]-3,5-dimethoxybenzene, Fenirofibrate and 3-Iodo-L-thyronine are the major chemical compounds with higher area percentage of 15.83 % and a small contribution from amino groups of 2.91%.

CONCLUSIONS

The co-HTL process was performed for various process conditions proposed by Taguchi's method. The simulation results were predicted in terms of contour plot for pressure, temperature, HTC and heat flux distribution and compared with the experimental results. The maximum temperature and pressure of 589.3 K and 22.1 MPa were developed in run-8, which shows the corresponding deviation of 8.55 K and 1.3 MPa with experimental values. A wide range of temperature variation between casing and slurry biomass was observed from 1.9 to 3.4% in simulation and 1.3 to 1.5% in experimental values. The lower particle density and higher process temperature were two main reasons for the minimum temperature difference and led to effective heat transfer in run-8. Likewise, runs 8 and 1 delivered the maximum and minimum HTC of 6001 W/m^2K and 5760 W/m^2K in simulation, which have respective deviations of 5.6% and 4.2% with experimental values. Hence, the lower particle density, higher water-to-biomass ratio, mass flow rate and process temperature are suitable process conditions for efficient heat transfer between the reaction chamber and biomass slurry.

The overall energy recovery of 70.8% was attained at higher process temperature, mass flow rate and the water-to-biomass ratio of 595 K, 0.007 kg/s, 8.3 and lower PP biomass mixture of 4:1. Similar process conditions were recommended to obtain higher HHV of 45.9 MJ/kg and 32.69 MJ/kg for corresponding biochar and bio-crude. It also provided a higher H/C ratio for biochar and biocrude of 1.13 and 1.93, respectively. The predicted HHV revealed the maximum deviations of 15.7% and 12.6% from the actual HHV for respective biochar and bio-crude. In the case of bioproduct yield, the moderate temperature of 575 K provided the maximum yields of biochar as 45.3% and biocrude as 53.2% at their respective water-to-biomass ratios of 6.3 and 8.3. In addition, the biochar exhibited a synergetic effect up to 575 K at a 4:1 biomass mixture and the higher temperature led to an antagonistic effect. Likewise, the synergetic effect in bio-crude was noticed at a lower PP biomass ratio irrespective of process temperatures. Based on percentage selectivity, bio-liquids attained from run-5, run-8 and run-9 proceeded for GC-MS analysis, run-8 had a higher proportion of light oxygenated compounds as 17.2% and aromatic hydrocarbons of 10.34%. 1-[(E)-2-(4-chlorophenyl) ethenyl]-3,5-dimethoxybenzene, 2-Methoxyphenol ($C_7H_8O_2$) and Phenol (C_6H_5OH) were the major aromatic hydrocarbons found in bio-crude. In both heat transfer and performance studies, it is recommended that the process conditions given in run-8 were suggested to recover the maximum energy from the biomass and to attain effective heat transfer.

In the future, the hydraulic pump with a capacity of 40 MPa can be utilized to operate under high process temperature and pressure. It will also assist in improving thermal degradation and expect better conversions of bioproducts.

MATERIALS

Table 1. Proximate and ultimate analysis of dried PJ and PP (textile packing waste)

Feed stock	H (%)	C (%)	N (%)	S (%)	O (%)	HHV (MJ/kg)	Volatile matter (%)	Moisture (%)	FC (%)	Ash (%)
PJ	7.1	48.3	0.4	1.6	42.6	20.5	77.4	7.9	13.2	1.5
PP	14.7	85.3	-	-	-	46.1	87.2	10	2.8	-

Table 2. HHV in MJ/kg for different ratios of PJ and PP (dry basis) using a bomb calorimeter

PJ to PP ratio	1:0	1:1	1:4	4:1	0:1
HHV in MJ/kg	21.8	42.28	51.18	44.64	45.52

The co-liquefaction of Prosopis juliflora (PJ) and textile packaging waste (containing 98% polypropylene) was utilized in the hydrothermal process. The PJ was obtained from wasteland and chopped into fine mesh sizes of 60-80 in the local sawmill. Table 1 shows the characterization analysis of both PJ and PP performed in an elemental analyzer and tubular furnace. Similarly, the HHV of PJ and PP at different ratios was calculated using temperature differences obtained from the oxygen-type bomb calorimeter, as given in Table 2. The highest HHV of 51.18 MJ/kg was estimated for a 1:4 PJ to PP biomass ratio and the lowest HHV of 21.8 was obtained for PJ biomass. As a result of incomplete combustion in PP, the HHV of the biomass mixture at 1:4 was higher than the HHV of polypropylene (45.52 MJ/kg). Zhiwei Wang et al.,[30] confirmed that the presence of PJ could enhance the combustion efficiency and leading to the complete combustion of the volatile components in PP. The PP has attained the heat of fusion state and undergoes phase changes during the combustion. When it was mixed with PJ, the heat released from these phase changes and the combustion of PJ can be contributed to a higher HHV. The interaction between the melting PP and the combusting PJ can lead to more efficient heat transfer and higher overall energy release [30].

EXPERIMENTAL SECTION

Experimental setup

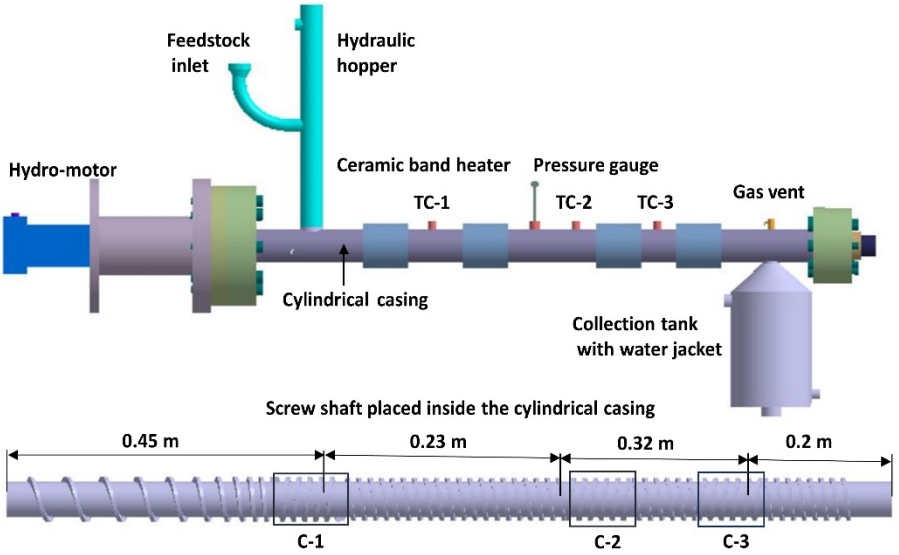

Figure 8. 3D model of hydraulically actuated continuous high-pressure screw reactor

The co-HTL process was carried out in a high-pressure Archimedes screw reactor with a 3L internal volume and heated using two ceramic band heaters, as shown in Fig. 8. The screw shaft was designed for optimal design parameters such as a screw diameter of 58 mm, helix angle of 6.8°, pitch and flight length of 29 mm and 1200 mm, respectively. It is enclosed within a stationary cylindrical casing having a thickness of 16 mm. TC-1, TC-2 and TC-3 are the thermocouples fixed at three different locations on the casing, shown in Fig. 7 to measure the temperatures of slurry biomass inside the reactor. The high torque hydraulic motor (H15) was attached to the screw shaft, which rotates at a speed ranging from 60 to 90 rpm. The piston-type hydraulic hopper was fixed to the inlet side of the reactor for injecting the biomass. It also prevents back pressure from developing at the beginning of the first compression zone. The storage tank was integrated with the water-cooling jacket and coupled at the outlet end of the reactor. Similarly, the sample collection ports were available at the bottom of each compression zone. Finally, the reaction pressure was measured at the mid-section of the reactor with the help of a pressure gauge.

Experimental Procedure

The ideal combinations of process parameters, including temperatures, feed rates and water-to-biomass ratios, were obtained from Taguchi's experimental design, as given in Table 3. Initially, the feedstock was prepared for three different biomass ratios of PJ and PP including 4:1, 1:1 and 1:4. A wide range of water-to-biomass ratios were selected, from 6.3 to 8.3 for preparing 1kg of biomass slurry. Then, the prepared biomass was loaded into the reaction chamber at atmospheric condition with a feed rate ranging from 20 to 30 kg/h. The additional deionized water was injected through the water nozzle to avoid clogging near the compression zones during the flow of biomass. The continuous process took a retention time of 60 to 120 minutes to reach the biomass in the collection tank. The retention time was varied for each run due the restricted flow in the compression zone. The biomass was heated after passing the first compression zone for 363 K and the reaction temperature has been maintained between the second and third compression zones of the reactor. Finally, the processed material was collected in the storage tank and cooled for around 45 minutes to attain the atmospheric temperature.

Product separation technique

After the collected samples had cooled down to ambient conditions, acetone (50 mL) was added to the 200 g of samples. The vacuum filtration method was conducted for the separation of liquid and solid phases from the collected kerogen. Then, the solid residue was dried in the hot air oven at 333K for 8h to remove the presence of acetone and the dried solid product was weighed. Further, the aqueous phase (AqP) was separated from the organic phase (oil + solvent) using a separating funnel, thereby the rotary vacuum evaporator was introduced to separate the required biocrude from the acetone present in the organic phase. Finally, the recovered acetone was reused for other product separation processes. The yields of biosolid, biocrude and AqP were calculated under dry conditions using the given equations (1), (2) and (3). These values can also be applied to determine the co-liquefaction effect of biomass using Eq. (5).

$$Biosolid\ yield, Y_{BS}\ (\%) = \left(\frac{Mass\ of\ biochar}{Mass\ of\ combined\ feedstocks}\right) \times 100 \quad (1)$$

$$Biocrude\ yield, Y_{BC}\ (\%) = \left(\frac{Mass\ of\ biocrude}{Mass\ of\ combined\ feedstocks}\right) \times 100 \quad (2)$$

$$Biogas\ and\ AqP, Y_{BG,AqP}\ (\%) = 100 - (Y_{bs} + Y_{bc}) \quad (3)$$

Table 3. Experimental process parameters for co-HTL process from Taguchi's method

Runs	Temperature (K)	Feed rate (kg/h)	Water-to-biomass ratio	Biomass ratio (PJ/PP)	Capacity of water in mL, weight of PJ and PP in grams (g)	Additional water added (L)
1	555	20	6.3	04:01	733:213.6:53.4	0.95
2	555	25	7.3	01:01	1100:200:200	1.82
3	555	30	8.3	01:04	1466:106.8:427	2.97
4	575	20	8.3	01:01	733:133.5:133.5	1.48
5	575	25	6.3	01:04	1100:80:320	1.42
6	575	30	7.3	04:01	1466:427.2:106	2.43
7	595	20	7.3	01:04	733:53.4:213.6	1.22
8	595	25	8.3	04:01	1100:320:80	2.22
9	595	30	6.3	01:01	1466:267:267	1.89

Analytical methods

The direct gross calorific value or HHV of biomass mixtures, biochar and biocrude was evaluated using the oxygen bomb calorimeter. The 1g test sample was placed in the stainless-steel chamber and it was filled with pressurized oxygen at 300 bars. Thereafter, the initial and final temperature differences were observed to calculate the gross calorific value of the samples by applying equation (4).

The gross calorific value or HHV of biosolid (BS) and bio-crude (BC) was estimated using the given equation,

$$HHV_{BS\ or\ BC} = (3326.248 \times temperature\ difference) - [(60 \times 0.355) + (30 \times 4.18)] \quad (4)$$

The co-liquefaction effect of combined biomass based on biochar and biocrude yield was calculated by,

$$Co - liquefaction\ effect, (E_{CL}) = Y_{co-HTL} - \Sigma\, y_j \times x_j \quad (5)$$

Y_{co-HTL}= yield of biochar or biocrude from the co-liquefaction process; y_j= yield of individual biomass; x_j= mass fraction of respective biomass from the feedstock mixture.

The energy yield of biosolid and bio-crude was calculated according to Eqs. (6) and (7),

$$Energy\ yield\ of\ biosolid,\ EY_{Bs}\ (\%) = \frac{HHV_{Bs}}{HHV_{biomass}} \times Y_{Bs} \quad (6)$$

$$Energy\ yield\ of\ biocrude,\ EY_{BC}\ (\%) = \frac{HHV_{BC}}{HHV_{biomass}} \times Y_{BC} \quad (7)$$

The Dulong equation for calculating HHV of bioproducts is given by [27],

$$HHV = 0.338\,C + 1.44\,H - 0.18\,O + 0.095\,S \quad (8)$$

Simulation process condition

The bulk density, specific heat capacity, thermal conductivity and heat generation are the important thermal properties given in Table 4, which were used in the respective governing equations during CFD analysis. After fitting the initial values in the simulation, it computes the temperature and pressure distribution and HTC.

Table 4. Thermal properties of mixed biomass and process conditions applied in CFD simulations

Runs	Temperature (K)	Mass flow rate (kg/s)	Bulk density (kg/m^3)	Specific heat at constant pressure, Cp (J/kg-K)	Heat generation (W/m^3)	Thermal conductivity (W/mK)
1	555	0.005	933	3378	10840	0.5
2	555	0.007	899	3433	10840	0.5
3	555	0.0085	933	3270	10840	0.5
4	575	0.005	1052	3433	11230	0.5
5	575	0.007	899	3752	11230	0.5
6	575	0.0085	872	3378	11230	0.5
7	595	0.005	1080	3270	11620	0.5
8	595	0.007	872	3400	11620	0.5
9	595	0.0085	899	3433	11620	0.5

The continuity equations of fluid and solid phases based on mass balance are given by,

$$\frac{\partial}{\partial t}\varphi_f \rho_f + \nabla.\left(\varphi_f \rho_f u_f\right) = 0 \tag{9}$$

$$\frac{\partial}{\partial t}\varphi_s \rho_s + \nabla.\left(\varphi_s \rho_s u_s\right) = 0 \tag{10}$$

The momentum equations of fluid and solid with shear stress tensor and drag force are given by,

$$\frac{\partial}{\partial t}\varphi_f \rho_f u_f + \nabla.\left(\varphi_f \rho_f u_f u_f\right) = -\varphi_f \nabla p + \nabla \tau_f - \beta(u_f - u_s) + \varphi_f \rho_f g + \frac{N_p}{V} F_d \tag{11}$$

$$\frac{\partial}{\partial t}\varphi_s \rho_s u_s + \nabla.\left(\varphi_s \rho_s u_s u_s\right) = -\varphi_s \nabla p - \nabla p_s + \nabla \tau_s - \beta\left(u_f - u_s\right) + \varphi_s \rho_s g + \frac{N_p}{V} F_d \tag{12}$$

The thermal energy equation of fluid and solid phases is described as follows,

$$\frac{\partial}{\partial t}\left(\varphi_f \rho_f C_{Pf} T_f\right) + \nabla.\left(\varphi_f \rho_f C_{Pf} T_f u_f\right) = \nabla. q_f + h_{fs}\left(T_s - T_f\right) - \Delta H_f + h_{casing\ wall}\left(T_{casing\ wall} - T_f\right) \quad (20)$$

$$\frac{\partial}{\partial t}\left(\varphi_s \rho_s C_{Ps} T_s\right) + \nabla.\left(\varphi_s \rho_s C_{Ps} T_s u_s\right) = \nabla. q_s + h_{sf}\left(T_f - T_s\right) - \Delta H_s + h_{casing\ wall}\left(T_{casing\ wall} - T_s\right) \quad (21)$$

Whereas, conductive heat flux, $q_s = \varphi_s k_s \nabla T_s$

ACKNOWLEDGMENTS

This research article is based on CFD and performance analysis of continuous high-pressure screw reactors under various process conditions carried out by the authors. The authors would like to thank all the researchers who contributed to the research work. Throughout this study, the authors acknowledge Kongu Engineering College for their support of the research facility. The authors also thank IIT, madras and SAIF, cochin for their contribution to the respective GC-MS and elemental analysis on the test samples.

REFERENCES

1. J. Yang, Q. He and L. Yang, *Appl. Energ.*, **2019**, 250: 926-45.
2. F. Cheng, J.M. Jarvis, J. Yu, U. Jena, N. Nirmalakhandan, T.M. Schaub and C.E. Brewer, *Bioresource Technol.*, **2019**, 294: 122184-93.
3. I.A. Basar, H. Liu, H. Carrere, E. Trably and C. Eskicioglu, *Green Chem.,* **2021**, 23(4): 1404-46.
4. R.F. Beims, Y. Hu, H. Shui and C. Xu, *Biomass Bioenerg.*, **2020**, 135: 105510-24.
5. A. Aierzhati, J. Watson, B. Si, M. Stablein, T. Wang and Y. Zhang, *Energ. Convers. Man.-X*, **2021**, 10(1): 100076-86.
6. C. Jazrawi, P. Biller, A.B. Ross, A. Montoya, T. Maschmeyer and B.S. Haynes, *Algal Res.*, **2013**, 2(3): 268-77.
7. J. Ni, L. Qian, Y. Wang, B. Zhang, H. Gu, Y. Hu and Q. Wang, *Fuel*, **2022**, 327: 125135-49.
8. M. Tabatabaei, M. Aghbashlo, M. Dehhaghi, H.K.S. Panahi, A. Mollahosseini, M. Hosseini and M.M. Soufiyan, *Prog. Energy Combust. Sci.*, **2019**, 74(1): 239-303.

9. D.C. Elliott, T.R. Hart, G.G. Neuenschwander, L.J. Rotness, G. Roesijadi, A.H. Zacher and J.K. Magnuson, *ACS Sustain. Chem. Eng.,* **2013**, 2(2): 207-15.
10. I.M. Sintamarean, I.F. Grigoras, C.U. Jensen, S.S. Toor, T.H. Pedersen and L.A. Rosendahl, *Biomass Convers. Biorefin.,* **2017**, 7(4): 425-35.
11. D.W.F. Brilman, N. Drabik and M. Wądrzyk, *Biomass Convers. Biorefin.,* **2017**, 7(4): 445-54.
12. A.R. Suesse, G.A. Norton and J. van Leeuwen, *Energ. Fuel.*, **2016**, 30(9): 7379-86.
13. J.L. Wagner, C.D. Le, V.P. Ting and C.J. Chuck, *Fuel Process. Technol.,* **2017**, 165: 102-11.
14. W.T. Chen, M.A. Haque, T. Lu, A. Aierzhati and G. Reimonn, *Curr. Opin. Environ. Sci. Health,* **2020**, 14: 63-73.
15. K. Anastasakis, P. Biller, R. Madsen, M. Glasius and I. Johannsen, *Energies*, **2018**, 11(10): 2695-718.
16. T.H. Pedersen, I.F. Grigoras, J. Hoffmann, S.S. Toor, I.M. Daraban, C.U. Jensen, S.B. Iversen, R.B. Madsen, M. Glasius, K.R. Arturi, R.P. Nielsen, E.G. Søgaard and L.A. Rosendahl, *Appl. Energ.,* **2016**, 162: 1034-41.
17. C.U. Jensen, J.K. Rodriguez Guerrero, S. Karatzos, G. Olofsson and S.B. Iversen, *Biomass Convers. Biorefin.*, **2017**, 7(4): 495-509.
18. X. Shi, F. Ronsse, J. Roegiers and J.G. Pieters, *Renew. Energ.,* **2019**, 143: 1465-76.
19. X. Shi, F. Ronsse, R. Nachenius and J.G. Pieters, *Renew. Energ.,* **2019**, 143: 1477-87.
20. S. Aramideh, Q. Xiong, S.-C. Kong and R.C. Brown, *Fuel*, **2015**, 156(1): 234-42.
21. S. Jalalifar, R. Abbassi, V. Garaniya, F. Salehi, S. Papari, K. Hawboldt and V. Strezov, *Fuel*, **2020**, 273: 117782-96.
22. F. Qi and M.M. Wright, *Powder Technol.*, **2018**, 335: 18-34.
23. C. Sheng and J.L.T. Azevedo, *Biomass Bioenerg.,* **2005**, 28(5): 499-507.
24. Q. Liu, R. Xu, C. Yan, L. Han, H. Lei, R. Ruan and X. Zhang, *Bioresour. Technol*., **2021**, 340: 125630-40.
25. B. Li, T. Yang, R. Li and X. Kai, *Energy*, **2020**, 200: 117524-33.
26. H. Li, Z. Zhu, J. Lu, J. Watson, D. Kong, K. Wang, Y. Zhang and Z. Liu, *Fuel*, **2020**, 280: 118605-18.
27. A. Mathanker, D. Pudasainee, A. Kumar and R. Gupta, *Fuel*, **2020**, 271: 117534-44.
28. D. Mahesh, S. Ahmad, R. Kumar, S.R. Chakravarthy and R. Vinu, *Bioresour. Technol*., **2021**, 339: 125537-47.
29. J.S. dos Passos, S. Chiaberge and P. Biller, *Energ. Fuel,* **2021**, 35(13): 10630-40.
30. Z. Wang, Y. Chen, G. Chen, T. Sun, M. Zhang, Q. Wang, M. Wu, S. Guo, S. Yang, T. Lei, K.G. Burra and A.K. Gupta, *J. Energy Resour. Technol.*, **2023**, 145(8): 1-8.
31. X. Tao and C.A. Infante Ferreira, Int. J. Heat Mass Tran., **2019**, 135: 996-1012.
32. S. Mukundan, J.L. Wagner, P.K. Annamalai, D.S. Ravindran, G.K. Krishnapillai and J. Beltramini, *Fuel Process Technol.,* **2022**, 238: 107523-32.

33. C.D. Venkatachalam, M. Sengottian, S.R. Ravichandran, K. Subramaniyan and P. Kalappan Thangamuthu, *Period. Polytech. Chem. Eng.,* **2020**, 65(1): 105-15.
34. M.S. Seshasayee and P.E. Savage, *Appl. Energ.*, **2020**, 278: 115673-85.
35. J.S. dos Passos, M. Glasius and P. Biller, *Process Saf. Environ.,* **2020**, 139: 371-79.
36. W.-T. Chen, K. Jin and N.-H. Linda Wang, *ACS Sustain. Chem. Eng.,* **2019**, 7(4): 3749-58.
37. S. Hongthong, S. Raikova, H.S. Leese and C.J. Chuck, *Waste Manage.,* **2020**, 102: 351-61.
38. N. Li, H. Liu, Z. Cheng, B. Yan, G. Chen and S. Wang, *J. Hazard Mater.,* **2022**, 424: 127460-72.
39. J.A. Onwudili and P.T. Williams, *J. Clean. Prod.*, **2023**, 430: 139733-46.
40. X. Zhang, L. Zhang and A. Li, *Bioresource Technol.*, **2019**, 294: 122113-22.